REDUCTION OF LASER-INDUCED CHOROIDAL NEOVASCULARIZATION BY INTRAVITREAL VASOHIBIN-1 IN MONKEY EYES

HIDEYUKI ONAMI, MD,*† NOBUHIRO NAGAI, PHD,* SHIGEKI MACHIDA, MD,‡ NORIHIRO KUMASAKA, MS,* RYOSUKE WAKUSAWA, MD,† YUMI ISHIKAWA, MS,* HIKARU SONODA, PHD,§ YASUFUMI SATO, MD,¶ TOSHIAKI ABE, MD*

Purpose: To determine whether intravitreal vasohibin-1 will reduce the grade of the choroidal neovascularization in monkey eyes.

Methods: Choroidal neovascularizations were induced in 12 monkey eyes by laser photocoagulation. Three monkeys were evaluated for the safety of the vasohibin-1 injections, 6 monkeys for the effects of a single injection, and 3 monkeys for repeated injections of vasohibin-1. Ophthalmoscopy, fluorescein angiography, focal electroretinograms, and optical coherence tomography were used for the evaluations. The level of vascular endothelial growth factor in the aqueous was determined by enzyme-linked immunosorbent assay. Immunohistochemistry was performed.

Results: An intravitreal injection of 10 μg of vasohibin-1 induced mild intraocular inflammation. Eyes with an intravitreal injection of 0.1 μg and 1.0 μg of vasohibin-1 had significant less fluorescein leakage from the choroidal neovascularizations and larger amplitude focal electroretinograms than that of vehicle-injected eyes. Similar results were obtained by repeated injections of 0.1 μg of vasohibin-1. Immunohistochemistry showed that vasohibin-1 was expressed mainly in the endothelial cells within the choroidal neovascularizations. The vascular endothelial growth factor level was not significantly altered by intravitreal vasohibin-1.

Conclusion: The reduction of the laser-induced choroidal neovascularizations and preservation of macular function in monkey by intravitreal vasohibin-1 suggest that it should be considered for suppressing choroidal neovascularizations in humans.

RETINA X:1–10, 2012

Age-related macular degeneration (AMD) is one of the most common sight-threatening disease in developed countries.[1] A choroidal neovascularization (CNV) is a typical finding in eyes with the wet-type AMD, and the CNV can lead to subretinal hemorrhages, exudative lesions, serous retinal detachment, and disciform scars.[2] Many different types of treatments have been used to treat AMD, for example, laser photocoagulation,[3] surgery,[4,5] transpupillary thermotherapy,[6] photodynamic therapy,[7] and intravitreal injection of anti–vascular endothelial growth factor (VEGF).[8,9] Each of these treatments has advantages and disadvantages, and the best treatment of AMD has still not been determined.

Different pro- and antiangiogenic factors play important roles in the development and progression of CNVs.[10] Among the proangiogenic factors, VEGF has been shown to play a major role.[11] Thus, anti-VEGF therapy is being used to successfully treat CNVs in patients with AMD.[8,9] However, this method requires repeated injections that can lead to irritation, infection, and other adverse side effects.[12] In addition, not all patients respond to the therapy.[13] Thus, other types of therapy need to be developed to treat AMD eyes with a CNV.

Vasohibin-1 is a VEGF-inducible molecule expressed by human cultured endothelial cells (ECs) and has antiangiogenic properties.[14] Its expression is selectively induced in ECs not only by VEGF but also by several other proangiogenic factors such as basic fibroblast growth factor.[15] Vasohibin-1 inhibits the formation of EC networks in vitro, corneal neovascularization,[14] and retinal neovascularization in a mouse model of oxygen-induced ischemic retinopathy.[16] Vasohibin-1 is found in the vitreous and in

proliferative membranes of patients with diabetic retinopathy. The level of vasohibin-1 is significantly correlated with the VEGF level in the vitreous of patients with proliferative diabetic retinopathy.[17] Vasohibin-1 is also expressed in the CNV membranes of patients with AMD.[18] Eyes with lower vasohibin-1/VEGF expression ratios tend to have larger CNV lesions, whereas those with higher vasohibin-1/VEGF ratios have subretinal fibrosislike lesions.[18]

We have found that the laser-induced CNVs were less active in mice injected intravitreally with vasohibin-1 than those injected with the vehicle.[19] Thus, the purpose of this study was to determine the effect of intravitreal vasohibin-1 on the laser-induced CNVs in monkey eyes. We shall show that the intravitreal vasohibin-1 was safe and reduced the degree of the CNVs in monkey eyes.

Methods

Animals

The procedures used in the animal experiments followed the guidelines of the The Association for Research in Vision and Ophthalmology Statement for the Use of Animals in Ophthalmic and Vision Research, and they were approved by the Animal Care Committee of Tohoku University Graduate School of Medicine. Twelve Japanese macaque monkeys (*Macaca fuscata*) between ages 4 and 6 years and weighing between 4.2 kg and 10.1 kg were used (Table 1). For all procedures, the monkeys were anesthetized with an intramuscular injection of ketamine hydrochloride (35 mg/kg) and xylazine hydrochloride (5 mg/kg), and the pupils were dilated with topical 2.5% phenylephrine and 1% tropicamide. Oxybuprocaine hydrochloride (0.4%) was also used for local anesthesia. Three monkeys were used to evaluate the safety of intravitreal vasohibin-1, 6 monkeys for dose dependency of a single injection of vasohibin-1, and 3 monkeys for repeated injections of vasohibin-1.

Table 1. Monkey Eyes Used in This Study

	Vasohibin (mg)	Number of Eyes	Inflammation
Nontreated	0	1	0/1
	0.01	1	0/1
	0.1	1	0/1
	1	1	0/1
	10	1	1/1
	100	1	1/1
Laser application	0	3	0/3
	0.01	3	0/3
	0.1	3	0/3
	1	3	1/3
Laser application	0	3	0/3
	0.1	3	0/3
Total		24	3/24

Inflammation shows clinical inflammation signs that were observed during the experiments.

Experimental Choroidal Neovascularization

An argon green laser was used to rupture of the choroidal membrane using a slit-lamp delivery system (Ultima 2000SE; Lumenis, Yokneam, Israel) with a contact lens.[20] The laser settings were as follows: 50-μm diameter, 0.1-second duration, and 650-mW to 750-mW intensity. Five laser burns were made around the macula within 15° of the fovea. The foveola was not treated. Each burn was confirmed to have induced subretinal bubbles indicating a rupture of Bruch membrane.

Expression and Purification of Human Vasohibin-1 Polypeptide

Human vasohibin-1 was purified from *Escherichia coli* as described.[21] Human vasohibin-1 was isolated as a thioredoxin fusion protein. The fusion protein was dialyzed and digested with blood coagulation Factor Xa (Novagen, Darmstadf, Germany). The released vasohibin-1 was collected, eluted, and dialyzed against 20 mM glycine–HCl buffer (pH 3.5). Then, the vasohibin-1 was resolubilized with 50 mM Tris–HCl buffer containing 50 mM NaCl, 5 mM tris(2-carboxyethyl)phosphine, 0.5 mM ethylenediaminetetraacetic acid, 5% glycerol, and 4.4% *N*-lauroylsarcosine (pH 8.0) and was dialyzed against 20 mM sodium phosphate buffer at pH 8.0. This buffer was also used as the vehicle.

The protein concentration was determined by the Bradford method with a protein assay kit (Bio-Rad Laboratories, Hercules, CA), with bovine serum albumin as a standard protein.

From the *Division of Clinical Cell Therapy, United Center for Advanced Medical Research and Development; †Department of Ophthalmology and Visual Science, Graduate School of Medicine, Tohoku University, Miyagi, Japan; ‡Department of Ophthalmology, Iwate Medical University, Iwate, Japan; §Diagnostic Division, Shionogi & Co., Ltd. Osaka, Japan; and ¶Department of Vascular Biology, Institute of Development, Aging, and Cancer, Tohoku University Graduate School of Medicine, Miyagi, Japan.

Supported in part by grants from Grants-in-Aid for Scientific Research 21592214 and 20592030 (to T. Abe) from the Japan Society for the Promotion of Science, Chiyoda-ku, Tokyo, Japan and by Suzuken Memorial Foundation.

This study was performed at the Tohoku University. Monkeys were supplied by National BioResource Project for breeding and supply.

The authors declare no conflict of interest.

Reprint requests: Toshiaki Abe, MD, Division of Clinical Cell Therapy, United Center for Advanced Research and Translational Medicine (ART), Graduate School of Medicine, Tohoku University, 1-1 Seiryoumachi Aobaku Sendai, Miyagi, 980-8574 Japan; e-mail: toshi@oph.med.tohoku.ac.jp

Intravitreal Injection of Recombinant Vasohibin-1 Polypeptide

Vasohibin-1 was injected intravitreally in 3 groups of monkeys (Table 1). The first group of 6 eyes did not have a laser burn and received a single injection of vehicle, or 0.01, 0.1, 1, 10, or 100 μg of vasohibin-1/50 μL of vehicle. The second group of 12 eyes of 6 monkeys (3 eyes for each concentration) received a single injection of vehicle or 0.01, 0.1, and 1 μg of vasohibin-1/50 μL of vehicle 4 days after the laser burn. The third group of 3 eyes had 3 injections of 0.1 μg of vasohibin-1/50 μL of vehicle in the right eyes and 50 μL of vehicle in 3 fellow eyes on 0, 4, and 7 days after the laser burn. We examined the natural course of laser-induced CNVs in mice, and the CNVs were most active around Day 14 after the laser burn, and then gradually regressed, especially 28 days after laser burn. When we injected vasohibin-1 into the vitreous of mice after laser burns, we found that the injection of vasohibin-1 on Day 4 after the laser burn was most effective, followed by Days 7 and 1. Other days were less effective. In addition, immunohistochemical studies for vasohibin-1 in the mouse CNV membranes showed that the later the laser burn, the more vasohibin-1 staining was observed.[19] So we decided to do the repeated vasohibin-1 injections on 0, 4, and 7 days after the laser burn (relatively early days after laser burn).

For the intravitreal injections, the monkeys were anesthetized and pupils were dilated. The intravitreal injections were made with a 30-gauge needle attached to a 1-mL syringe. The needle was inserted through the sclera into the vitreous cavity ~1.5 mm posterior to the limbus while observing the eye with an operating microscope. The fundus was examined after the injection to confirm that the retina and lens were not damaged.

Ophthalmic Examinations

In addition to the routine ophthalmologic examinations, fluorescein angiography (FA) with an imaging system (GENESIS-Df; Kowa, Tokyo, Japan), optical coherence tomography (OCT, RS3000; NIDEK, Tokyo, Japan), and focal and full-field electroretinography (ERG) were performed on the selected days. Fluorescein angiography was performed 1, 2, and 4 weeks after the laser photocoagulation. Two retinal specialists (R.W. and T.A.) graded the angiograms in a masked way using a grading system[22]: Grade 1, no hyperfluorescence; Grade 2, hyperfluorescence without leakage; Grade 3, hyperfluorescence in the early or middle phase and leakage in the late phase; and Grade 4, bright hyperfluorescence in the transit and leakage in late phase beyond the treated areas.

The central macular thickness was determined from the macular thickness maps (3.45 mm in diameter) of the scans by OCT 4 weeks after the laser photocoagulation. The volume of the lesion was also calculated using the same program.

The pupils were maximally dilated for the ERG recordings 4 weeks after intravitreal vasohibin-1 injections. The ERGs were amplified and digitally bandpass filtered from 0.5 Hz to 500 Hz for the full-field ERGs and from 5 Hz to 500 Hz for the focal ERGs (PuREC; Mayo, Aichi, Japan). The animals were dark adapted for at least 30 minutes before the full-field ERG recordings. The light for the stimulus was obtained from light-emitting diodes (EW-102; Mayo Co., Nagoya, Japan) embedded in a contact lens electrode. The intensity and duration of the stimuli were controlled by an electronic stimulator (WLS-20; Mayo Co.). Chlorided silver plate electrodes were placed on the forehead and right ear lobe as reference and ground electrodes, respectively. The intensity of the stimulus was 1,000 cd/m^2 and the duration was 3 milliseconds.

Focal ERGs were recorded 4 weeks after the laser photocoagulation with a focal ERG system (PuREC; Mayo; ER-80; Kowa) that was integrated into an infrared fundus camera. This system was developed and described in detail by Miyake et al.[23,24] The stimulus spot was 15° in diameter and was placed on the macula by viewing the ocular fundus on a monitor. The intensity of the stimulus was 1,000 cd/m^2, and the background light was 1.5 cd/m^2. The stimulus duration was 100 milliseconds. A Burian–Allen bipolar contact lens electrode (Hansen Ophthalmic Laboratories, Iowa City, IA) was inserted into the anesthesized conjunctival sac to record the focal ERGs. A chlorided silver electrode was placed on the left ear lobe as the ground electrode. Two hundred to 300 responses were averaged at a stimulation rate of 5 Hz.

The a-waves were measured from the baseline to the trough of the first negative response, and the b-wave from the first trough to the peak of the following positive wave. The amplitudes of a-waves and b-waves from the three untreated monkeys were used as control. The number of monkeys used in this experiment was not added to the total number of monkeys.

Immunohistochemistry

Immunostaining for vasohibin-1was done on eyes with laser-induced CNVs 28 days after the laser application. From the results of CNV experiments on

mice,[19] the laser-induced CNV lesions were self-resolved >28 days after the laser burn. Thus, we decided to enucleate the eyes 28 days after the laser burn, although there may be differences between mice and monkeys. The eyes were enucleated and fixed in 4% paraformaldehyde overnight, and the anterior segment and lens were removed. The posterior segment was embedded in paraffin, and 3-μm serial sections were cut, and adjacent sections were stained with hematoxylin and eosin.

The immunohistochemical staining for vasohibin-1 was performed with the peroxidase method and for cytokeratin by the alkaline phosphatase method. Mouse monoclonal antibodies against vasohibin-1 (1:400) and mouse monoclonal anti-pan cytokeratin (1:200; Sigma-Aldrich, St. Louis, MO) were applied to the sections overnight at 4°C. Then the sections were incubated in biotin-conjugated anti-mouse immunoglobulin (Histfine SAB-PO(M) kit; Nichirei, Tokyo, Japan). The slides for vasohibin were incubated with peroxidase-conjugated streptavidin (Histfine SAB-PO(M) kit; Nichirei), and the slides for cytokeratin were incubated with alkaline phosphatase–conjugated streptavidin (Histfine; Nichirei). HistoGreen (HISTOPRIME HistoGreen substrate kit for peroxidase; Ab Cys SA) was used for the chromogen of vasohibin, and VECTOR RED (alkaline phosphatase substrate kit 1; Vector, Burlingame, CA) was used for the chromogen of cytokeratin. The slides were counterstained with hematoxylin. For control, preimmune mouse immunoglobulin G was used instead of the primary antibody.

Enzyme-Linked Immunosorbent Assay for Vascular Endothelial Growth Factor

Aqueous was collected by a 30-gauge needle from the anterior chamber of each monkey 4 weeks after the laser photocoagulation. The level of the VEGF peptide was quantified by enzyme-linked immunosorbent assay according to the manufacturer's instructions (R & D Systems, Mckinley, MN; Quantikine Human VEGF immunoassay) using 50 μL of aqueous. The intensity of the color of the reaction products was measured with a MAXline microplate reader (Molecular Devices Corporation, Palo Alto, CA). The measurements were made in duplicate, and the mean was used. The concentration of VEGF was expressed as the amount of protein in picograms per milliliter (pg/mL).

Statistical Analyses

Analysis of variance with Scheffe test for post hoc analysis was used to examine the differences in the leakage and intensity of the CNVs in the fluorescein angiograms, amplitudes of the ERGs, mean central thickness, and volume of the CNV. The differences were also compared using the Student two-sample *t*-tests.

Results

Safety Evaluations and Outcomes

Before any of the procedures, the retina and choroid were normal in all the monkeys. Then 6 nontreated eyes were injected intravitreally with vehicle or 0.01, 0.1, 1, 10, or 100 μg of vasohibin-1/50 μL. After 0.01, 0.1, and 1 μg of vasohibin-1, the appearance of the retina and choroid did not differ from that of the vehicle-injected eyes. When 10 μg or 100 μg/50 μL of vasohibin-1 polypeptide was injected, a mild inflammation (Grade 1)[25] was detected in the vitreous on the day after the injection. The inflammation was less with 10 μg than with 100 μg of vasohibin, and the inflammation was resolved in 2 days after 10 μg and in 1 week after 100 μg (Table 1). When we injected 1 μg/50 μL of vasohibin-1 once in the laser-treated eyes, 1 of the 3 eyes developed inflammation in the aqueous. An inflammation was not observed when 0.1 μg of vasohibin-1 was injected even after 3 injections. When we injected 50 μL of vehicle with almost the same amount of endotoxin (400 U/mL) as that of 100 μg of vasohibin-1, no inflammation was detected. These results indicated that mild inflammation can develop with $\geq$10 μg of vasohibin-1 injection into the vitreous in nontreated monkey eyes.

The amplitudes of the a- and b-waves of the full-field ERGs of eyes injected with 0.01 μg to 100 μg of vasohibin-1 did not differ significantly from the vehicle-injected eyes. The a-wave amplitudes ranged from 87.3 μV to 180.3 μV (average, 119.3 ± 36.6 μV) before and from 100.7 μV to 195.8 μV (average, 131.3 ± 53.7 μV; $P = 0.444$) after the vasohibin-1 injection. The b-wave amplitudes ranged from 219.6 μV to 340.6 μV (average 250.6 ± 54.7 μV) before and from 240.8 μV to 345.2 μV (average 274.4 ± 82.0 μV, $P = 0.801$) after the vasohibin-1 injection.

Effect of Different Concentrations of Vasohibin-1

After the laser photocoagulation, we injected vehicle or 0.01, 0.1, or 1 μg of vasohibin-1/50 μL of vehicle in 3 eyes of each dosage for a total of 12 eyes (Table 1). From the results of safety evaluations, we selected the maximum amount of vasohibin-1 as 1 μg of vasohibin-1/50 μL of vehicle. Representative results of FA at 1, 2, and 4 weeks after the laser application for each dose of vasohibin-1 are shown in Figure 1. Color fundus photographs and focal ERGs recorded at 4 weeks are also shown.

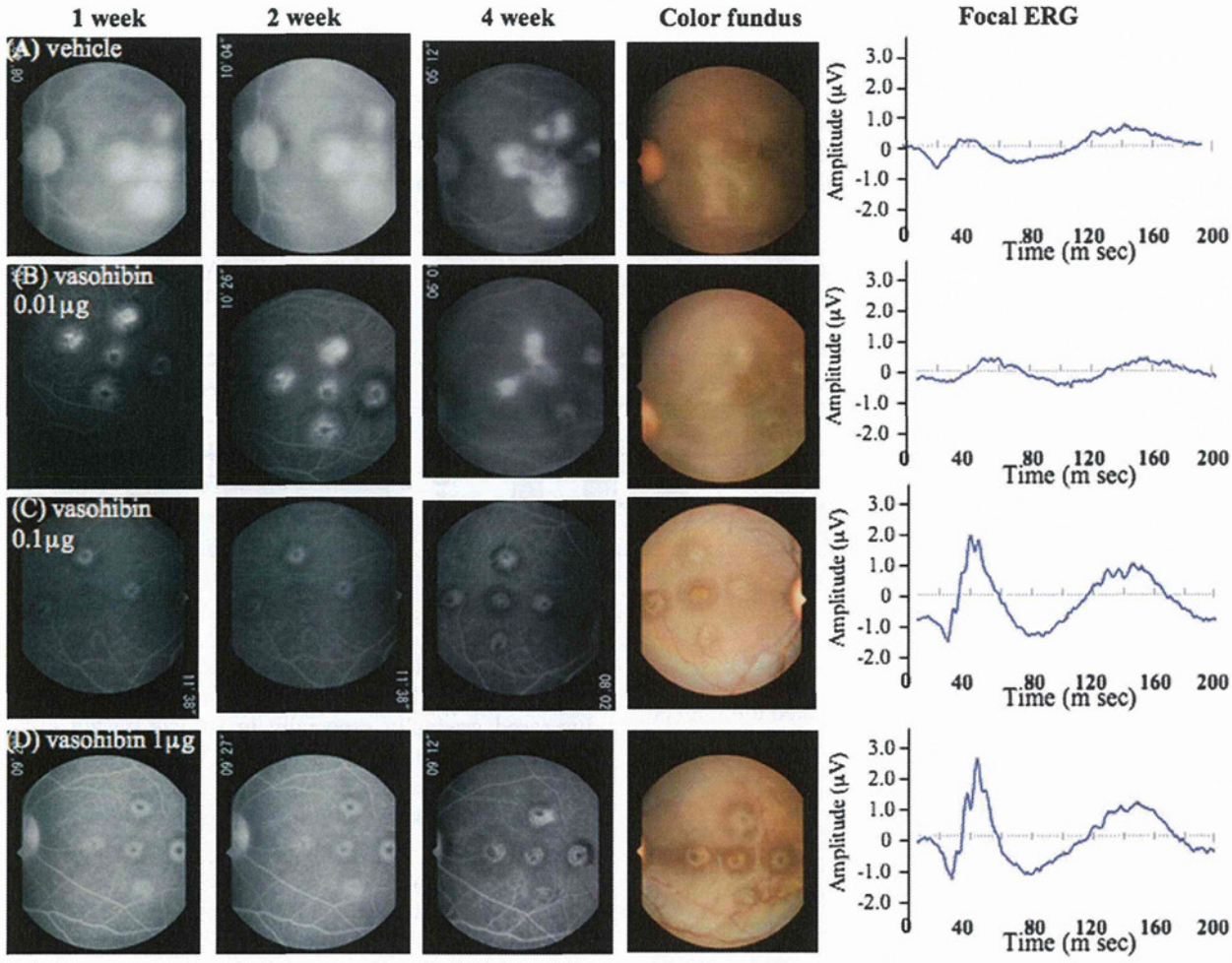

COLOR

Fig. 1. Representative FAs, fundus photographs, and focal ERGs from 6 monkey eyes are shown. Vehicle or 0.01, 0.1, 1 μg of vasohibin-1/50 μL of vehicle was injected intravitreally, and representative results at 1, 2, and 4 weeks after laser treatment are shown (see quantitative values in Figure 2, A–D). The FA images are those at around 10 minutes after the fluorescein injection. Color fundus photographs were taken 4 weeks after the laser application. Focal ERGs recorded 4 weeks after the laser photocoagulation are shown in the right column for each eye.

The CNV activity was scored using the FA grading system[22] for all five laser spots in each eye. The FA score for each spot was summed and compared with each other (Figure 2A). Our findings showed that there was significantly less leakage after 0.1 μg of vasohibin-1 than that for vehicle ($P = 0.016$) and for 0.01 μg ($P = 0.035$) of vasohibin-1 at 1 week. Significantly less leakage after 0.1 μg of vasohibin-1 than that of vehicle was also observed at 4 weeks ($P = 0.0307$). Because 1 μg of vasohibin-1 showed mild inflammation in 1 eye, we did not analyze the CNV in these eyes. The percentage of eyes with FA scores of 4 is also listed in Figure 2B. Our results showed that 45% of vehicle-treated eyes had Grade 4 leakage, and it was 45% in 0.01 μg of vasohibin-1–treated eyes, 7% with 0.1 μg of vasohibin-1–treated eyes, and none in the 1-μg vasohibin-1–treated eyes (only 2 eyes) at 1 week. Similarly, the percentage of eyes with Grade 4 leakage was 27%, 13%, 7%, and 0% at 2 weeks and 20%, 20%, 0% and 0% at 4 weeks after the vasohibin-1 injection (Figure 2B).

The amplitudes of the a-waves of the focal ERGs after 0.01 μg of vasohibin-1 were significantly smaller than those of the controls ($P = 0.041$) (Figure 2C). The amplitudes of the b-waves of the focal ERG b amplitudes in the vehicle-injected eyes ($P = 0.0085$) and in the 0.01-μg vasohibin-1–injected eye ($P = 0.0184$) were significantly smaller than those of the controls (Figure 2D). The results of inflammation, FA leakage, and ERG amplitudes led us to select 0.1 μg of vasohibin-1 as the optimal concentration for intravitreal injection to reduce the laser-induced CNV in our monkeys.

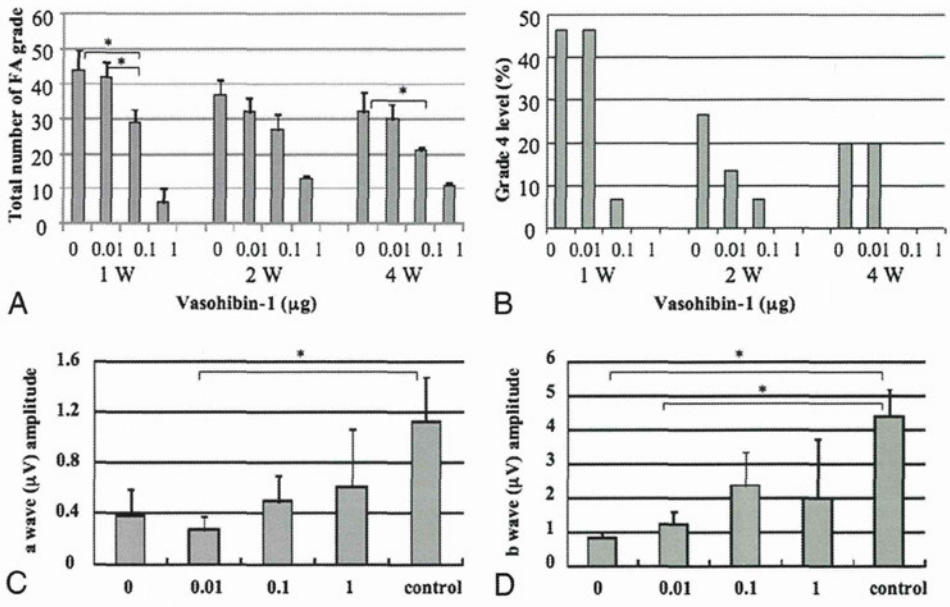

Fig. 2. Fluorescein angiographic scores for each of the 5 laser spots in each eye are plotted for each group, and the amplitudes of the a- and b-waves of the focal ERGs. **A.** Fluorescein angiographic scores for each of the five laser spots in each eye are plotted for each group. Statistically significant differences are shown as asterisks. **B.** Distribution of Grade 4 FA scores for each group is shown. **C** and **D.** Average amplitude of the a-waves (**C**) and b-waves (**D**) of the focal ERG recorded 4 weeks after intravitreal vasohibin-1. Vehicle (0) or 0.01, 0.10, or 1.00 μg of vasohibin-1 was injected in control eyes or eyes after the laser burns. Untreated controls show the effects before laser treatment. The averages ± standard deviations of the amplitudes of the a- and b-waves are plotted on the ordinate.

Effects of Repeated Injections of Vasohibin-1

Next, we examined the effects of repeated intravitreal injections of 0.1 μg of vasohibin-1/50 μL of vehicle in the right eyes on 0, 4, and 7 days after the laser application while the fellow eyes received an injection of the vehicle on the same days. We studied three eyes in each group. Representative fundus photographs, FAs, and OCT images after vehicle alone are shown in Figure 3 (A and B) and after 0.1 μg of vasohibin-1/50 μL of vehicle in Figure 3 (C and D). The FA scores were significantly lower in the vasohibin-1–injected eyes than in the vehicle-injected eyes at 4 weeks (P = 0.009; Figures 3 and 4A). At 1 week and 2 weeks after the vasohibin-1 injections, the FA scores were not significantly different (P = 0.07). The percentage of eyes scored as Grade 4 was 13.3% at 1 week, 26.7% at 2 weeks, and 26.7% at 4 weeks in the vehicle-treated eyes, whereas no Grade 4 eyes were observed in the 0.1 μg of vasohibin-1/50 μL of vehicle-treated eyes at any time (Figure 4B).

Although statistical significance was not observed in the a-wave amplitude of the focal ERGs, statistically significant larger b-wave amplitudes were observed in the vasohibin-1–treated eyes than that of vehicle (P = 0.039) (Figure 4, C and D).

Optical coherence tomography examinations showed that the retinal pigment epithelium and Bruch membrane were disrupted in the laser-treated eyes at 1 week and 2 weeks after the laser application (Figure 3, B and D) as was found in histologic preparations.[22] At 4 weeks, an retinal pigment epithelium–like membrane appeared over the CNV lesion (Figure 3, B and D). This line was shown to be cytokeratin positive. The OCT images showed that the size of the CNV increased gradually especially in vehicle-treated eyes as was seen in the FA images.

Optical coherence tomography also showed that the macular thickness (Figure 4E) and volume (Figure 4F) of the CNV lesions after 0.1 μg of vasohibin-1/50 μL of treated eyes was ~30% less than the vehicle-treated eyes in the central 1 mm. When we examined the volume of the central 6 mm, no difference was observed between the vasohibin-1–treated and vehicle-treated eyes.

Histology and Immunostaining of Choroidal Neovascularization

Histopathologic analyses showed that the retina and choroid surrounding the CNV had normal architecture in both the vehicle and vasohibin-1–treated eyes as reported.[26] The vehicle-treated eyes after the laser application showed a disruption of the Bruch membrane and retinal pigment epithelium complex, and the eyes had different degrees of fibrous tissues and vessels (Figure 5, C and E). Eyes treated with vasohibin-1 tended to have smaller CNV than that of vehicle-treated eyes.

Cytokeratin labeling demonstrated that retinal pigment epithelial cells from the edges of the wound had proliferated and covered the laser wound to different degrees. Although a disruption of the cytokeratin labeling was present in the vehicle-treated eyes (Figure 5, D and F), we could not find any significant difference from that of the vasohibin-1–injected eyes. Different

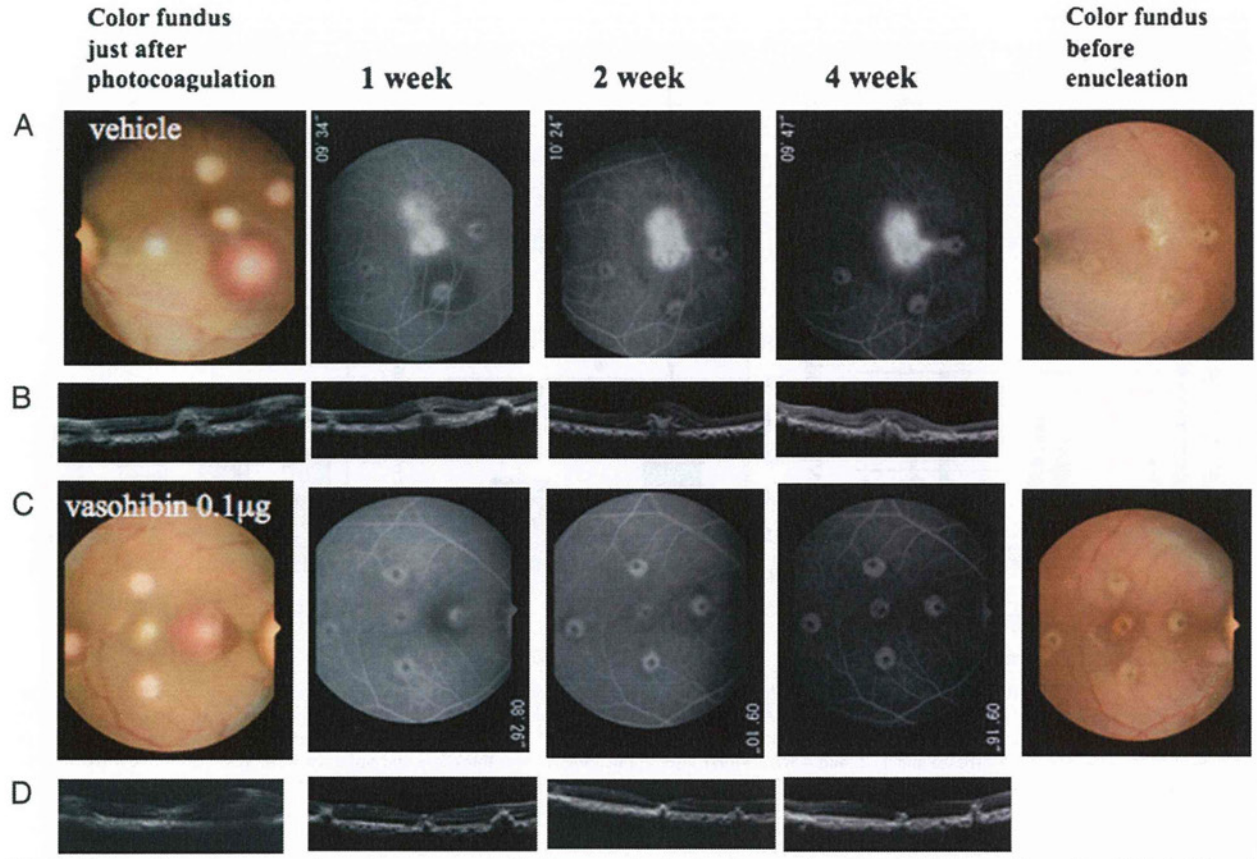

COLOR

Fig. 3. Fluorescein angiograms, ocular coherence tomographic images, color fundus photographs, and focal ERGs are shown. Vasohibin-1 (0.1 μg/50 μL) was injected into the vitreous of the right eyes 3 times on 0, 4, and 7 days after laser application, and the same amount of vehicle was injected into left eyes on the same days. Photographs show the fundus just after the laser application and the day of enucleation. Fluorescein angiographs recorded 1, 2, and 4 weeks after laser application. Photographs of the right (**A**) and left (**C**) eyes are shown. The results of OCT on the indicated days are shown in the same vertical columns for the indicated day (**B**) and (**D**).

numbers of macrophage-like cells were also observed in the neural retina.[21]

In immunostained eyes, vasohibin-1 positivity was found mainly in the CNV especially on the ECs in the CNV (Figure 5B). The regions surrounding the CNV showed little vasohibin-1–positive staining. Some monkeys showed no vasohibin-1 expression by immunohistochemistry even in the CNV at 28 day after laser application. Positive staining for vasohibin-1 appeared to be greater in the more active CNVs (Figure 5A), and it was more obvious in nontreated monkey eyes, although we could not determine whether the staining was significantly greater because only 3 monkey eyes were studied.

Vascular Endothelial Growth Factor in Aqueous During Experiments

The level of VEGF was determined by enzyme-linked immunosorbent assay. The average VEGF level in the aqueous in the vasohibin-1–injected eyes was 15.3 pg/mL, and it was 20.6 pg/mL in the vehicle-treated eyes at 4 days after laser application. The average VEGF level in the vasohibin-1– and vehicle-treated eyes were 7.0 pg/mL and 8.9 pg/mL, respectively, at 4 weeks after laser application (Figure 6). For both times, the differences were not significant.

Discussion

Our results demonstrated that when 10 μg or 100 μg of vasohibin-1 was injected intravitreally into nontreated normal monkey eyes, a mild anterior chamber inflammation developed. No signs of inflammation or any adverse effects were found when <1 μg of vasohibin-1 was injected into nonlaser treated eyes, although we used only 1 eye for each dose. However when 1 μg of vasohibin-1 was injected into laser-treated eyes, a mild inflammation developed in 1 of the 3 eyes. Inflammation has also been reported in monkey

COLOR

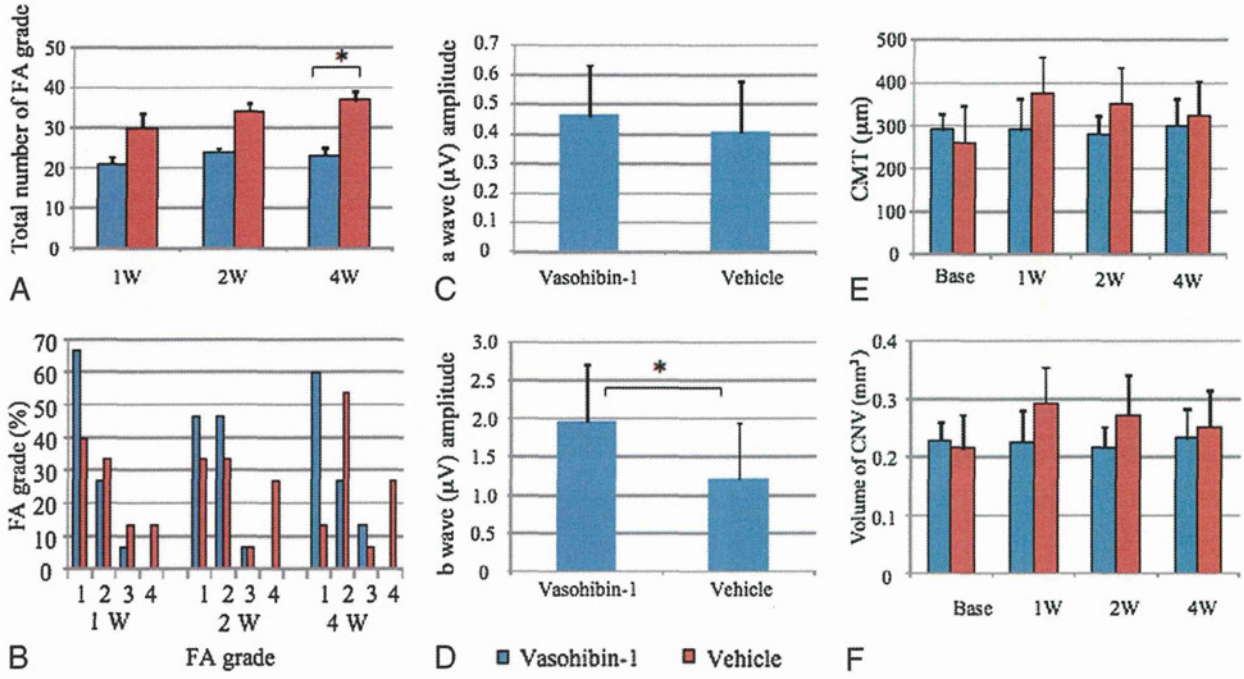

Fig. 4. Results of FA, focal ERG, and OCT are shown. **A.** Significantly less FA leakage was observed after 0.1 μg/50 μL of vasohibin-1 than after vehicle treatment at 4 weeks. **B.** Distribution of Grade 4 FA eyes for each group. **C** and **D.** Average amplitudes of the a-waves (**C**) and b-waves (**D**) of the focal ERGs. **E** and **F.** Average central macular thickness (CMT) and the central 3.4 mm and volume of area of either vasohibin-1–treated (blue) or vehicle-treated (red) eyes before (base) and 1, 2, and 4 weeks after laser application. Lower thickness and volumes were observed in the vasohibin-1–treated monkeys. Data are the standard deviations.

eyes after intravitreal injections of fragments of mouse and human chimera antibodies against VEGF.[22,27]

Fluorescein angiography examination after vasohibin-1 injection in laser-treated eyes showed significantly lower FA scores in eyes that received 0.1 μg and 1 μg of vasohibin-1 than the vehicle-injected eyes, although the number of eyes may have affected the statistics. Fluorescein leakage from the laser spots close to the macula was greater than that of the other laser spots. These results are compatible with the results of Shen et al,[28] who also found that the laser spot was larger and the leakage was greater for lesions closer to the macula. We also found that fluorescein leakage was different among monkeys, even though we applied the same amount of vasohibin-1.[22] This variability may be because the body weight ranged from 4.1 kg to 10.1 kg and age from 4 years to 6 years among the monkeys.

After we injected 0.1 μg of vasohibin-1 3 times in the right eyes and vehicle into the left eyes of 3 monkeys, we found significantly less fluorescein leakage in the vasohibin-1–treated right eyes than in the vehicle-treated eyes. The results of focal ERGs and OCT were well correlated with the results of FA findings, although the quantitative values were not significantly different.

Taken together, these results showed that intravitreal vasohibin-1 is able to reduce the activity of the laser-induced CNV in monkeys. With 3 injections of 0.1 μg of vasohibin-1, the results were not so different from that of only 1 injection at 4 days after the laser application. This may indicate that there may be an optimum time for the vasohibin-1 to affect the course of the laser-induced CNV. Alternatively, the results may be related to the half-life of vasohibin-1.

We found that vasohibin-1 was expressed on ECs especially those in the CNV lesions. Careful examinations showed that vasohibin-1 expression was limited to the CNV lesion and may not show extensive expression in other regions under normal physiologic conditions. Although we have not followed the expression of vasohibin-1 during the course of CNV development in monkeys, vasohibin-1 expression may be enhanced in the new vessels as was reported.[29] The vasohibin-1 expression appeared stronger in non-treated monkey eyes, although this could not be quantified. Vasohibin-1 has been reported to be present on the ECs only in the stroma of tumors and not in the noncancerous regions of the tissue in surgically resected tissues of the same patient.[29] These findings suggest that vasohibin-1 may be expressed mainly in the new vessels as it was in our laser-induced CNVs.

COLOR

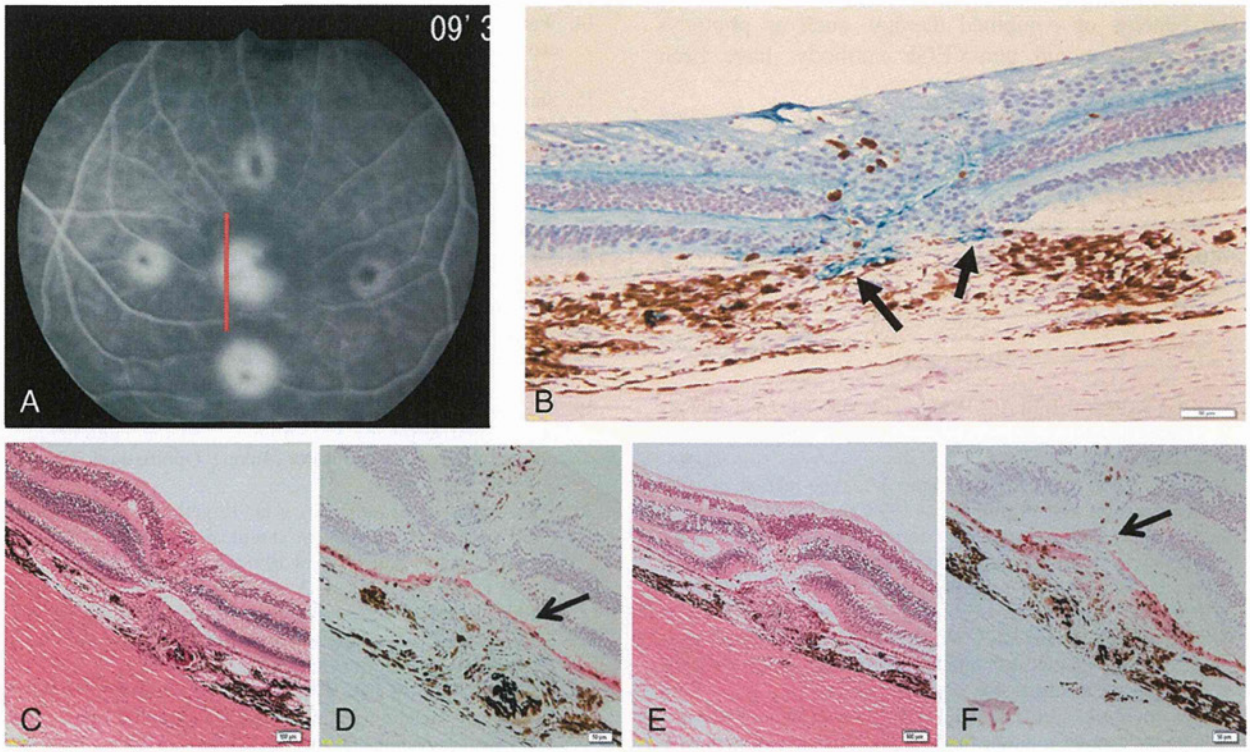

Fig. 5. Fluorescein angiograms 4 weeks after laser application or vehicle injection are shown. **A.** Immunohistochemistry for vasohibin-1 (**B**), the same eye as shown in (**A**) at the red line, is shown. Arrows indicate vasohibin-1 labeling. Vasohibin-1 expression is concentrated on the vessels around the CNV (arrows), but markedly less than in the CNV. Vaoshibin-1 expression was observed at active CNV (red line in **A**). The subretinal space is an artifact of histologic processing. Cytokeratin labeling is also shown with vasohibin-treated eye (**D**) and vehicle-treated eye (**F**). Arrows show labeling of cytokeratin. Bar = 50 μm. **C** and **E.** Hematoxylin and eosin staining of vasohibin-1–treated and vehicle-treated eyes, respectively, are shown. Bar = 100 μm. Cytokeratin labeling shows that retinal pigment epithelium covers CNV in the vasohibin-1–treated eyes (**D**), and a disruption of cytokeratin labeling is observed in vehicle-treated eye (**F**).

Hosaka et al[29] reported that exogenous vasohibin-1 blocked angiogenesis and maturation of not only the cancerous tissue but also the surrounding vessels and, thus, enhanced the antitumor effects of vasohibin-1. Intravitreal injection of vasohibin-1 may also suppress angiogenesis in CNVs by the same mechanism.

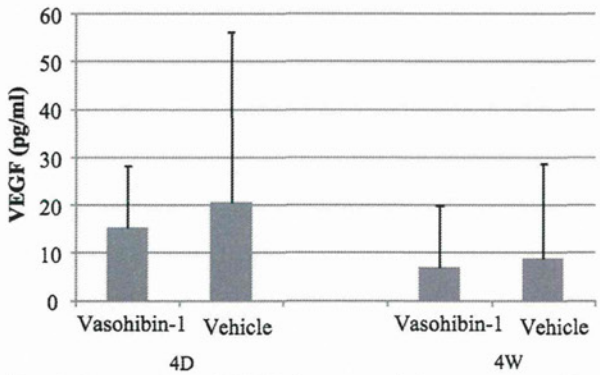

Fig. 6. Concentration of VEGF in aqueous in laser-treated monkey eyes 4 days and 4 weeks after laser application is shown. Vertical axis shows VEGF concentration in picograms per milliliter, and horizontal axis is the day of examination. Vascular endothelial growth factor in vasohibin-1–treated eyes (blue boxes) and vehicle-treated eyes (red boxes) show no significant difference at any times.

The amount of VEGF in the aqueous in the vasohibin-1–treated eyes did not differ from that in vehicle-treated eyes. Thus, Zhou et al[30] reported that external vasohibin-1 had no effect on the level of VEGF when they used adenovirus encoding human vasohibin-1 on mouse corneal neovascularization induced by alkali burn. They also reported that vasohibin-1 may downregulate the VEGF receptor 2 (VEGFR2). Shen et al[16] also reported a downregulation of VEGFR2 by vasohibin-1 during mouse ischemic retinopathy. Our previous studies have also shown a downregulation of VEGFR2 by external vasohibin-1 in laser-induced mouse CNVs.[19] Thus, vasohibin-1 may reduce the activity of a CNV by partially downregulating VEGFR2 in the eyes. If this is correct, vasohibin-1 may not affect the favorable aspects of VEGF such as its neuroprotective effect,[31] especially if VEGF works through VEGFR1 rather than VEGFR2. Vasohibin-1 also can be used with anti-VEGF antibody for CNV therapy.

The benefits of combined therapy, such as photodynamic therapy and anti-VEGF antibody, have been discussed.[27]

In conclusion, intravitreal vasohibin-1 in monkey eyes is safe and can reduce the activity of laser-induced CNVs and thus preserve the function of the macula.

Key words: choroidal neovascularization, laser-induced, monkey, vascular endothelial growth factor, vasohibin-1.

References

1. Klein R, Peto T, Bird AC, Vannewkirk MR. The epidemiology of age-related macular degeneration. Am J Ophthalmol 2004; 137:486–495.
2. Bressler NM, Bressler SB, Fine SL. Age-related macular degeneration. Surv Ophthalmol 1998;32:375–413.
3. Argon laser photocoagulation for neovascular maculopathy. Three-year results from randomized clinical trials Macular Photocoagulation Study Group. Arch Ophthalmol 1986;104: 694–701.
4. Thomas MA, Grand MG, Williams DF, et al. Surgical management of subfoveal choroidal neovascularization. Ophthalmology 1992;99:952–968.
5. Eckardt C, Eckardt U, Conrad HG. Macular rotation with and without counter-rotation of the globe in patients with age-related macular degeneration. Graefes Arch Clin Exp Ophthalmol 1999;237:313–325.
6. Reichel E, Berrocal AM, Ip M, et al. Transpupillary thermotherapy of occult subfoveal choroidal neovascularization in patients with age-related macular degeneration. Ophthalmology 1999; 106:1908–1914.
7. Photodynamic therapy of subfoveal choroidal neovascularization in age-related macular degeneration with verteporfin: one year results of 2 randomized clinical trials-TAP report Treatment of Age-related Macular Degeneration with Photodynamic Therapy (TAP). Study Group. Arch Ophthalmol 1999;117:1329–1345.
8. Grisanti S, Tatar O. The role of vascular endothelial growth factor and other endogenous interplayers in age-related macular degeneration. Prog Retin Eye Res 2008;27:372–390.
9. Miller JW, Adamis AP, Shima DT, et al. Vascular endothelial growth factor/vascular permeability factor is temporally and spatially correlated with ocular angiogenesis in a primate model. Am J Pathol 1994;145:574–584.
10. Krzystolik MG, Afshari MA, Adamis AP, et al. Prevention of experimental choroidal neovascularization with intravitreal anti-vascular endothelial growth factor antibody fragment. Arch Ophthalmol 2002;120:338–346.
11. Rosenfeld PJ, Brown DM, Heier JS, et al. Ranibizumab for neovascular age-related macular degeneration. N Engl J Med 2006;355:1419–1431.
12. Pilli S, Kotsolis A, Spaide RF, et al. Endophthalmitis associated with intravitreal anti-vascular endothelial growth factor therapy injections in an office setting. Am J Ophthalmol 2008;145:879–882.
13. Lux A, Llacer H, Heussen FMA, Joussen AM. Non-responders to bevacizumab (Avastin) therapy of choroidal neovascular lesions. Am J Ophthalmol 2007;91:1318–1322.
14. Watanabe K, Hasegawa Y, Yamashita H, et al. Vasohibin as an endothelium-derived negative feedback regulator of angiogenesis. J Clin Invest 2004;114:898–907.
15. Shimizu K, Watanabe K, Yamashita H, et al. Gene regulation of a novel angiogenesis inhibitor, vasohibin, in endothelial cells. Biochem Biophys Res Commun 2005;327:700–706.
16. Shen J, Yang X, Xiao WH, et al. Vasohibin is up-regulated by VEGF in the retina and suppresses VEGF receptor 2 and retinal neovascularization. FASEB J 2006;20:723–725.
17. Sato H, Abe T, Wakusawa R, et al. Vitreous levels of vasohibin-1 and vascular endothelial growth factor in patients with proliferative diabetic retinopathy. Diabetologia 2009;52:359–361.
18. Wakusawa R, Abe T, Sato H, et al. Expression of vasohibin, an antiangiogenic factor, in human choroidal neovascular membranes. Am J Ophthalmol 2008;146:235–243.
19. Wakusawa R, Abe T, Sato H, et al. Suppression of choroidal neovascularization by vasohibin-1, vascular endothelium-derived angiogenic inhibitor. Invest Ophthalmol Vis Sci 2011;52:3272–3280.
20. Tobe T, Ortega S, Luna JD, et al. Targeted disruption of the FGF2 gene does not prevent choroidal neovascularization in a murine model. Am J Pathol 1998;153:1641–1646.
21. Heishi T, Hosaka T, Suzuki Y, et al. Endogenous angiogenesis inhibitor vasohibin1 exhibits broad-spectrum antilymphangiogenic activity and suppresses lymph node metastasis. Am J Pathol 2010;176:1950–1958.
22. Krzystolik MG, Afshari MA, Adamis AP, et al. Prevention of experimental choroidal neovascularization with intravitreal anti-vascular endothelial growth factor antibody fragment. Arch Ophthalmol 2002;120:338–346.
23. Miyake Y, Yanagida K, Yagasaki K, et al. Subjective scotometry and recording of local electroretinogram and visual evoked response. System with television monitor of the fundus. Jpn J Ophthalmol 1981;25:439–448.
24. Kondo M, Ueno S, Piao CH, et al. Comparison of focal macular cone ERGs in complete-type congenital stationary night blindness and APB-treated monkeys. Vision Res 2008;48: 273–280.
25. Hogan MJ, Kimura SJ, Thygeson P. Signs and symptoms of uveitis. I. Anterior uveitis. Am J Ophthalmol 1959;47:155–170.
26. Zhang M, Zhang J, Yan M, et al. Recombinant anti-vascular endothelial growth factor fusion protein efficiently suppresses choroidal neovascularization in monkeys. Mol Vision 2008;14:37–49.
27. Husain D, Kim I, Gauthier D, et al. Safety and efficacy of intravitreal injection of ranibizumab in combination with verteporfin PDT on experimental choroidal neovascularization in the monkey. Arch Ophthalmol 2005;123:509–516.
28. Shen WY, Lee SY, Yeo I, et al. Predilection of the macular region to high incidence of choroidal neovascularization after intense laser photocoagulation in the monkey. Arch Ophthalmol 2004;122:353–360.
29. Hosaka T, Kimura H, Heishi T, et al. Vasohibin-1 expression in endothelium of tumor blood vessels regulates angiogenesis. Am J Pathol 2009;175:430–439.
30. Zhou SY, Xie ZL, Xiao O, et al. Inhibition of mouse alkali burn induced-corneal neovascularization by recombinant adenovirus human vasohibin-1. Mol Vision 2010;16:1389–1398.
31. Alon T, Hemo I, Itin A, et al. Vascular endothelial growth factor acts as a survival factor for newly formed retinal vessels and has implications for retinopathy of prematurity. Nat Med 1995;1:1024–1028.

Chapter 40
Vasohibin-1 and Retinal Pigment Epithelium

Yumi Ishikawa, Nobuhiro Nagai, Hideyuki Onami, Norihiro Kumasaka, Ryosuke Wakusawa, Hikaru Sonoda, Yasufumi Sato, and Toshiaki Abe

Keywords Vasohibin • VEGF • Retinal pigment epithelium • Hypoxia • Cell dynamics • Cobalt chloride

40.1 Introduction

Choroidal neovascularization (CNV) leads to subretinal hemorrhages, exudative lesions, serous retinal detachment, and disciform scars in patients with age-related macular degeneration (AMD) (Bressler et al. 1998). Vascular endothelial growth factor (VEGF), a pro-angiogenic factor, plays a major role in the development of CNV (Spilsbury et al. 2000). Recently, anti-VEGF treatment for patients with AMD has developed and reported good results (Krzystolik et al. 2002; Rosenfeld et al. 2006). However, there are many problems, such as repeated intravitreal injections, side effects (Pilli et al. 2008), suppression of the important physiological VEGF function (Alon et al. 1995), and further not all patients respond well to this therapy (Lux et al. 2007). Vasohibin-1 is a VEGF-inducible gene in human cultured endothelial cells (ECs) with antiangiogenic properties (Watanabe et al. 2004; Sonoda et al. 2006). Vasohibin-1 is induced by several pro-angiogenic factors such as VEGF and

Y. Ishikawa • N. Nagai • H. Onami • N. Kumasaka • R. Wakusawa • T. Abe (✉)
Division of Clinical Cell Therapy, United Center for Advanced Research and Translational Medicine (ART), Tohoku University Graduate School of Medicine, 1-1 Seiryoumachi Aobaku Sendai, Miyagi, Japan
e-mail: toshi@oph.med.tohoku.ac.jp

H. Sonoda
Discovery Research Laboratories, Shionogi and Co. Ltd. Osaka, Japan

Y. Sato
Department of Vascular Biology, Institute of Development, Aging, and Cancer, Tohoku University Graduate School of Medicine, Miyagi, Japan

M.M. LaVail et al. (eds.), *Retinal Degenerative Diseases*, Advances in Experimental Medicine and Biology 723, DOI 10.1007/978-1-4614-0631-0_40,

basic fibroblast growth factor (bFGF) (Watanabe et al. 2004). We showed that the vasohibin-1/VEGF ratio might play a role for clinical significance of CNV in patients with AMD using surgically excised CNV membranes (Wakusawa et al. 2008). The membranes included not only ECs but also retinal pigment epithelium (RPE). In this report, we examined the effects of vasohibin-1 on RPE.

40.2 Methods

40.2.1 RPE Preparation

We used commercially available rat RPE cell line, RPE-J. RPE-J was cultured in DMEM/F-12 medium with 4% fetal bovine serum (FBS; Sigma, St. Louis MO) with 5% CO_2 supply at 33°C. Human vasohibin-1 cDNA with antineomycin gene vector was transduced into RPE-J as we previously reported (Abe et al. 2008). Cells that were stably introduced the vector were selected by antibiotics. We selected 18 clones on both vasohibin-1 cDNA and only vector-transduced RPE-Js. Cobalt chloride (100–300 μM) and low glucose (0–100 μM) and oxygen supply (2%) were used for hypoxic stress. Vasohibin-1 was supplied from Shionogi and Co. Ltd, Osaka, Japan and VEGF and other chemicals were purchased from Wako (Tokyo Japan).

40.2.2 Real-Time RPE Impedance Analysis and MTS Assay

Dynamic cellular biology of the cultured RPE was monitored using Real-Time Cell Analyzer (RTCA), xCELLigence System (Roche Applied Science, Mannheim, Germany). The system evaluates cellular events in real time measuring electrical impedance at an electrode/solution interface at the bottom of cell culture plates. The system provides cell number, viability, morphology, and adhesion described as Cell Index (CI). RPE proliferation was also evaluated by 3-(4, 5-dimethylthiazol-2-yl)-5-(3-carboxymethoxyphenyl)-2-(4-sulfophenyl)-2H-tetrazolium, inner salt (MTS) assay, and counting cell number for each condition.

40.2.3 Extraction of mRNA, cDNA Generation, Reverse-Transcriptase, and Real-Time Polymerase Chain Reaction (RT-PCR)

mRNA was extracted and cDNAs were generated from the cells according to the manufacturer's instructions (Pharmacia Biotech Inc., Uppsala, Sweden). Semiquantitative real-time PCR was carried out by the primer sets described below (LightCycleST300:Roche, Basel, Swiss). The sequences were 5′-TCT GCT CTC

TTG GGT GCA AT-3′and 5′-TTC CGG TGA GAG GTC CGG TT-3′ for VEGF, 5′-GAT TCC CAT ACC AAG TGT GCC-3′ and 5′-ATG TGG CGG AAG TAG TTC CC-3′for vasohibin-1, and 5′-CATCACCATCTTCCAGGAGC-3′ and 5′-CATGAGTCCTTCCACGATACC-3′ for GAPDH. All data were normalized to the GAPDH expression level, thus giving the relative expression level.

40.2.4 Western Blot Analysis for Vasohibin-1 and VEGF

Cells were collected and used for western blotting analysis after sonication, as we reported previously (Abe et al. 2008). Cells were washed in ice-cold Dalbecco's phosphate buffered saline (DPBS) 3 times, and then immediately sonicated in lysis buffer. After blotting on Immune-Blot PVDF Membrane (BIO-RAD Laboratories, CA), it was incubated overnight in mouse antivasohibin-1 or anti-VEGF antibody (Santa Cruz) at 4°C and visualized using an enhanced chemiluminescence system (ECL Plus, GE Healthcare) according to the manufacturer's instructions.

40.3 Results

40.3.1 Vasohibin-1 Expression

Vasohibin-1 expression in the RPE was confirmed by real-time PCR and western blot analysis. When we cultured the cells with cobalt chloride, a pseudo-hypoxic condition, or low oxygen (2%), 1% serum, and no glucose, gradual upregulation of VEGF gene was observed with 100-μM cobalt chloride (Fig. 40.1a). Conversely, statistically significant low vasohibin-1 expression was observed with 100-μM cobalt chloride at more than 12-h culture when compared to those of standard culture or less than 6-h culture (Fig. 40.1b). Western blot analysis showed that vasohibin-1 expression seemed to be downregulated at more than 36-h culture with 100-μM cobalt chloride (Fig. 40.1c).

40.3.2 RPE Dynamics and Proliferation by Vasohibin-1

An RTCA was used to monitor dynamic changes in the properties of RPE cells during the culture. The parameter of CI shows cell viability, number, morphology, and adhesion to the bottom of the plates. When we cultured the cells under standard condition as described above, we found no difference of CI even though we added VEGF (Fig. 40.2a) and/or vasohibin-1 (Fig. 40.2b). When we added VEGF (0.2–10 nM) in the culture medium at 2% oxygen, 1% serum, and no glucose, we found that VEGF enhanced CI (Fig. 40.2c). Statistically significant difference was observed when we cultured the cells more than 15 h after treatments with 1 and 2-nM VEGF.

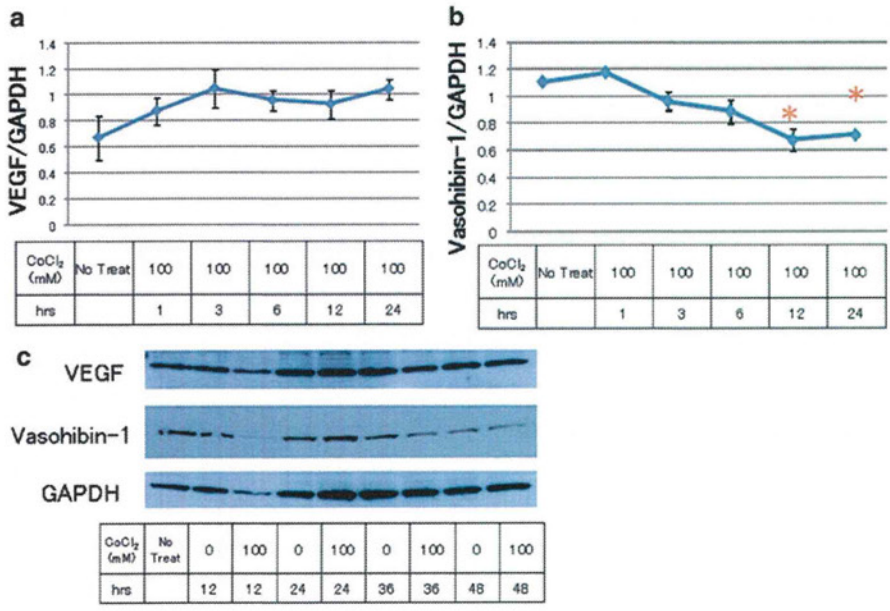

Fig. 40.1 Real-time PCR of VEGF (**a**) and vasohibin-1 (**b**) genes is shown. VEGF gene was upregulated in RPE-J with cobalt chloride during successive culture whereas vasohibin-1 gene was suppressed. Western blot analysis (**c**) shows decreased vasohibin-1 expression at the condition

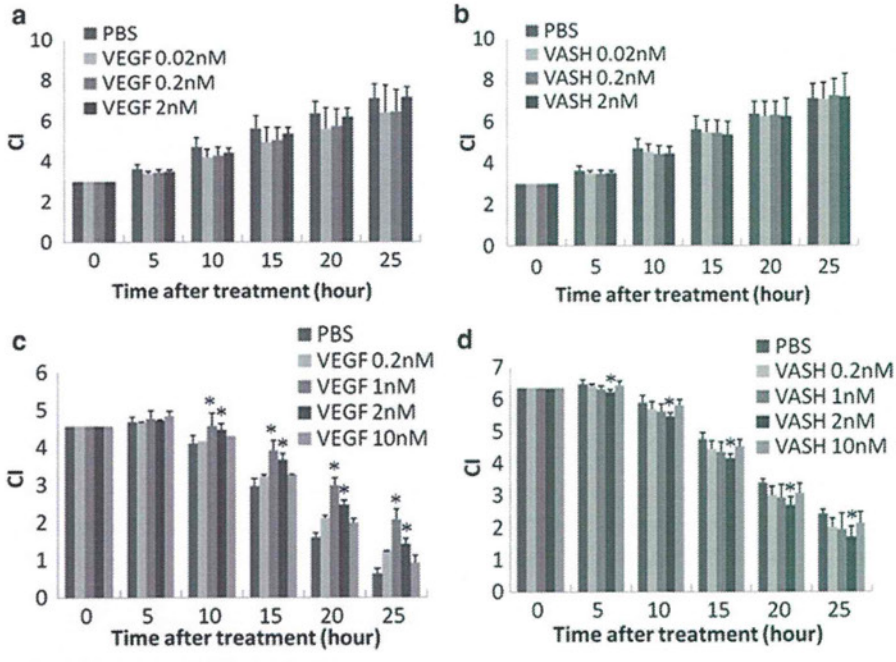

Fig. 40.2 Cell Index of RTCA shows that VEGF enhanced CI at hypoxic condition (**a**), conversely vasohibin-1 reduced CI only at hypoxic condition (**b**). The results were not observed at normal condition

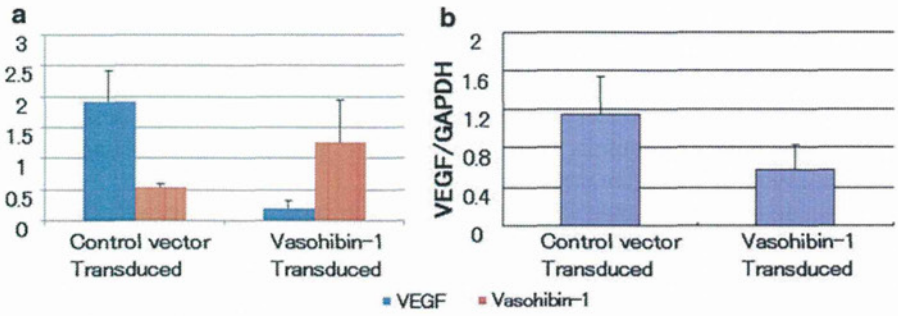

Fig. 40.3 Human vasohibin-1 gene was transduced into RPE-J. We selected 18 clones on both vasohibin-1 gene transduced and only vector-transduced RPE-J. Statistically significant less VEGF gene expression was observed in vasohibin-1 gene-transduced cDNA when compared to that of vector-transduced cDNA (**a**). Western blot analysis also showed comparable results (**b**)

Conversely, when we applied vasohibin-1 (0.2–10 nM) in the culture medium at 2% oxygen, 1% serum, and no glucose, we found that vasohibin-1 showed lower CI (Fig. 40.2d). Statistically significant difference was observed at 2-nM vasohibin-1. Vasohibin-1 application also showed statistically significant small cell number either 300-μM cobalt chloride or 2% oxygen, 1% serum, and no glucose. When we performed MTS assay, statistically significant less cell proliferation was also observed at these indicated conditions. When we examined the apoptotic cells, there was no significant difference. Human vasohibin-1 gene-transduced RPE-J showed statistically significant less VEGF expression when compared to those of vector-transduced cell by real-time PCR and western blot analysis (Fig. 40.3a, b).

40.4 Discussion

Vasohibin-1 is an endogenous antiangiogenic agent that is induced by variable pro-angiogenic factors such as VEGF and bFGF. Vasohibin-1 was reported to inhibit the sprouting of new vessels and to support vascular maturation processes (Kimura et al. 2009). These antiangiogenic properties were detected after recombinant vasohibin-1 was used for corneal and retinal neovascularization (Watanabe et al. 2004). We have found that vasohibin-1 is expressed on ECs of choroidal and retinal vessels, human CNV membranes (Wakusawa et al. 2008), and proliferative membranes of diabetic retinopathy (Sato et al. 2009). In addition, we suggested that the vasohibin-1/VEGF ratio was related to the activity of the CNV (Wakusawa et al. 2008). RPE is known for secreting VEGF from its basal side to choriocapillaris direction and performs important function for the survival of the vascular ECs and nonvascular cells developmentally and also in adults (Alon et al. 1995). This mechanism also maintains low VEGF concentration at subretinal space (Peng et al. 2010). Because of this specific function, we examined the correlation of vasohibin-1 and VEGF on RPE. From the results of present study, vasohibin-1 was expressed in RPE and the

expression was suppressed under hypoxic condition in RPE-J. Vasohibin-1 was also suspected to inhibit VEGF function of rat RPE. Interestingly, these results were observed only at hypoxic conditions and not in standard culture condition. Together with the previous reports, these results may show that vasohibin-1 may not suppress physiological VEGF function. External vasohibin-1 may participate as one of the molecules that suppress the pathological CNV.

In summary, we examined vasohibin-1 expression in rat RPE and the effects under normal or hypoxic condition. Vasohibin-1 expression was suppressed under hypoxic conditions. External vasohibin-1 plays an important role on RPE, especially in hypoxic condition, and suppresses VEGF function on rat RPE.

Acknowledgments This study was supported in part by grants from Grants-in-Aid for Scientific Research 20592030, 21592214 from the Japan Society for the Promotion of Science, Chiyoda-ku, Tokyo, Japan and Suzuken Memorial Foundation.

References

Abe T, Wakusawa R, Seto H et al (2008) Topical doxycycline can induce expression of BDNF in transduced retinal pigment epithelial cells transplanted into the subretinal space. Invest Ophthalmol Vis Sci 49: 3631–3639

Alon T, Hemo I, Itin A et al (1995) Vascular endothelial growth factor acts as a survival factor for newly formed retinal vessels and has implications for retinopathy of prematurity. Nat Med 1: 1024–1028

Bressler NM, Bressler SB, Fine SL (1998) Age-related macular degeneration. Surv Ophthalmol 32: 375–413

Kimura H, Miyashita H, Suzuki Y et al (2009) Distinctive localization and opposed roles of vasohibin-1 and vasohibin-2 in the regulation of angiogenesis. Blood 113: 4810–4818

Krzystolik MG, Afshari MA, Adamis AP et al (2002) Prevention of experimental choroidal neovascularization with intravitreal anti-vascular endothelial growth factor antibody fragment. Arch Ophthalmol 120: 338–346

Lux A, Llacer H, Heussen FMA et al (2007) Non-responders to bevacizumab (Avastin) therapy of choroidal neovascular lesions. Am J Ophthalmol 91: 1318–1322

Peng S, Adelman RA, Rizzolo LJ (2010) Minimal effects of VEGF and anti-VEGF drugs on the permeability or selectivity of RPE tight junctions. Invest Ophthalmol Vis Sci 51: 3216–33225

Pilli S, Kotsolis A, Spaide RF et al (2008) Endophthalmitis associated with intravitreal anti-vascular endothelial growth factor therapy injections in an office setting. Am J Ophthalmol 145: 879–882

Rosenfeld PJ, Brown DM, Heier JS et al (2006) MARINA Study Group. Ranibizumab for neovascular age-related macular degeneration. N Engl J Med 355: 1419–1431

Sato H, Abe T, Wakusawa R et al (2009) Vitreous levels of vasohibin-1 and vascular endothelial growth factor in patients with proliferative diabetic retinopathy. Diabetologia 52: 359–361

Sonoda H, Ohta H, Watanabe K et al (2006) Multiple processing forms and their biological activities of a novel angiogenesis inhibitor vasohibin. Biochem Biophys Res Commun 342: 640–646

Spilsbury K, Garrett KL, Shen WY et al (2000) Overexpression of vascular endothelial growth factor (VEGF) in the retinal pigment epithelium leads to the development of choroidal neovascularization. Am J Pathol 157: 135–144

Wakusawa R, Abe T, Sato H et al (2008) Expression of vasohibin, an antiangiogenic factor, in human choroidal neovascular membranes. Am J Ophthalmol 146: 235–243

Watanabe K, Hasegawa Y, Yamashita H et al (2004) Vasohibin as an endothelium-derived negative feedback regulator of angiogenesis. J Clin Invest 114: 898–907

Electrochemistry
The Electrochemical Society of Japan
Received: November 16, 2011
Accepted: February 4, 2012
Published: May 5, 2012
http://dx.doi.org/10.5796/electrochemistry.80.318
JOI:JST.JSTAGE/electrochemistry/80.318
Communication
Electrochemistry, **80(5)**, 318–320 (2012)

An Oxygen Responsive Microparticle-Patterned Hydrogel Sheet for Enzyme Activity Imaging

Kuniaki NAGAMINE,[a,b] Shuntaro ITO,[a] Mai TAKEDA,[a] Shingo OTANI,[a] and Matsuhiko NISHIZAWA[a,b,*]

[a] *Department of Bioengineering and Robotics, Graduate School of Engineering, Tohoku University, 6-6-01 Aramaki, Aoba-ku, Sendai 980-8579, Japan*
[b] *JST-CREST, Sanbancho, Chiyoda-ku, Tokyo 102-0075, Japan*

* *Corresponding author: nishizawa@biomems.mech.tohoku.ac.jp*

ABSTRACT
A patch-type oxygen imaging sheet useful for in vitro cellular metabolic assays was developed. Oxygen-responsive fluorescent microbeads were embedded into a biocompatible polyacrylamide gel sheet, which can be directly attached onto target cells for fluorescent imaging of metabolic activity. The sensor beads were directed in a microfluidic device using AC and DC electric manipulation techniques, followed by encapsulation in a hydrogel. Fluorescent imaging of oxygen-consuming activity was demonstrated for glucose oxidase-modified microparticles as cellular models to show the applicability of the imaging sheet to bioassays.

Keywords : Electrohydrodynamics, Microfluidic Device, Oxygen Imaging Sheet

1. Introduction

In vitro bioassays of cellular metabolic activity have been carried out to investigate the cell physiology. Evaluation of the oxygen-consuming activity of cells is significant for the indirect investigation of glucose metabolic activity. Such oxygen sensing would be applicable for revealing the mechanism of controlling blood glucose homeostasis and pathogenesis of type 2 diabetes using an insulin-responsive skeletal muscle cell.

In recent years, 2D fluorescent imaging sheets have been actively developed for mapping metabolite distribution in tissues.[1–4] In particular, Wolfbeis et al.[2,3] showed the applicability of pH- and oxygen-responsive sheets in animal experiments. All previous work used sheets in which the sensor microparticles were uniformly dispersed. However, the metabolite diffusion area is confined to the immediate vicinity of the cells. Besides, uniformly dispersed particles modify the characteristics of the hydrogel such as flexibility and nutrient permeability,[5] which will affect muscle cellular contractility and metabolic activity. In this study, the sensor beads were localized on the surface of the imaging sheet using AC and DC electric manipulation techniques to increase the surface sensitivity without sacrificing the merits of original gel characteristics. Fluorescent imaging of oxygen-consuming activity was demonstrated for glucose oxidase (GOD)-modified particles as cellular models (Fig. 1). When GOD-catalyzed glucose oxidation consumes the oxygen, the fluorescent intensity of the sensor beads increases in a pattern representing GOD activity.

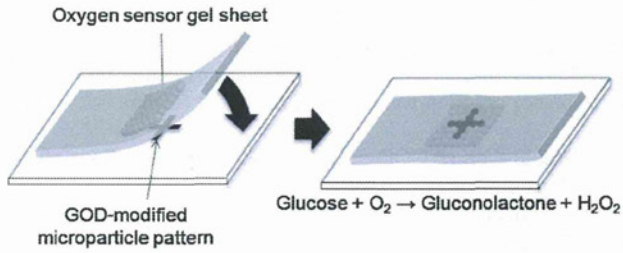

Figure 1. Schematic view of oxygen imaging around the pre-patterned GOD-modified microparticles.

2. Experimental

2.1 Preparation of oxygen responsive microparticles

A 3.5 mL of aqueous polystyrene microparticle suspension (1.0 μm diameter, Micromod) was mixed with 1.5 mL of tetrahydrofuran (THF) under ultrasonication for 10 min to swell the particles. A 0.5 mL solution of oxygen responsive fluorescent dye, platinum octaethylporphyrin (PtOEP, Sigma-Aldrich), dissolved in dimethyl sulfoxide was added to the particle suspension followed by another 20 min ultrasonication to incorporate the PtOEP into the particles.[6] Then, THF in the mixture was evaporated for 12 h at room temperature. The particles were separated by centrifugation, and washed two times with ethanol.

2.2 Fabrication of the microfluidic device

The microfluidic device was composed of three layers; an ITO top layer, a silicone rubber middle layer, and an ITO bottom layer covered with a negative photoresist SU-8 3005 pattern as an insulator. The silicone rubber layer had a stenciled opening that became the interior of the microchannel when sandwiched between the top and bottom ITO layers. The resulting microchannel was 10 mm in width and 500 μm in height. The channel inlet was connected to the particle suspension reservoir, and its outlet was attached to a syringe pump (World Precision Instruments) to introduce the particles into the channel.

2.3 Fabrication of the oxygen imaging sheet

The oxygen-responsive microparticles suspended in 0.5 mM NaCl solution were injected into the microchannel, and a sinusoidal AC voltage (100 Hz, 10 Vpp) was applied between the top and bottom ITO electrodes (Fig. 2A). The resulting AC electric field is strongest on the surface of the bottom ITO electrode, and the electrohydrodynamic force induces particle motion toward the bottom ITO pattern (1 mm × 1 mm). Then, the power supply was

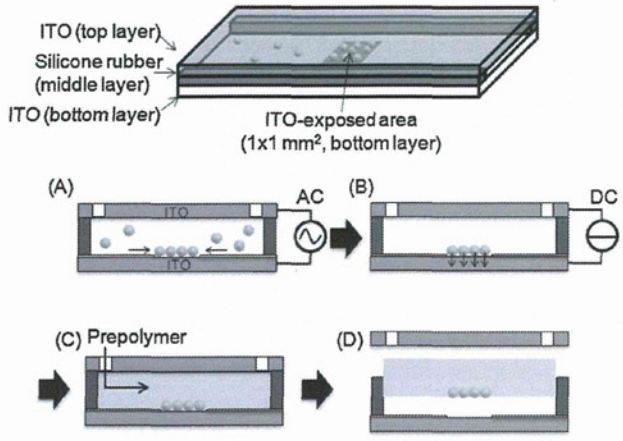

Figure 2. Preparation of the hydrogel sheet with patterned oxygen-responsive microparticles.

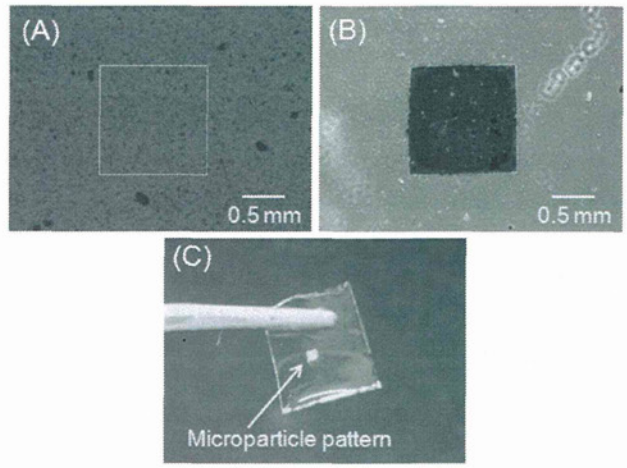

Figure 3. (A, B) Phase contrast micrographs (A) before and (B) after application of AC voltage between the top and bottom ITO electrodes. White-dashed line in (A) represents the ITO pattern on the bottom of the microchannel. (C) Photograph of the polyacrylamide hydrogel sheet with the oxygen responsive microparticle pattern embedded.

switched to 2.0 V DC to fix the patterned particles on the bottom ITO surface (Fig. 2B). After flushing out any unattached particles, the 20% (w/v) acrylamide and 1% (w/v) bis-acrylamide monomers including 0.4 vol% ammonium persulfate and 0.1 vol% tetramethylethylenediamine were injected into the channel. The device was left undisturbed for 2 h at room temperature to facilitate gelation (Fig. 2C).[7] The resulting sheet was cut into square (10 mm × 10 mm). The fluorescence of the particles was monitored using a fluorescent microscope (Olympus). The particles were excited at 520–550 nm using a mercury lamp and a bandpass filter, and a broad fluorescence emission was observed at around 650 nm.

2.4 Preparation of GOD-modified microparticle pattern on a glass substrate

Amino-functionalized microparticle suspension (1.0 μm diameter, Micromod) was dropped onto the stencil-attached amino-silanized glass substrate and evaporated overnight. The stencil sheet (100 μm thick) has a cross-formed line pattern (line width: 300 μm) made by a cutting plotter (Graphtech). An 8% glutaraldehyde solution was poured onto the particles for 1 h at room temperature to covalently immobilize the particles on the substrate and to functionalize the residual amines on the particles with glutaraldehyde. After washing away the unreacted glutaraldehyde, 1 mg/mL GOD (Wako Pure Chemicals Co.) suspended in PBS(−) (pH 7.0) was poured onto the particles and reacted at 4°C overnight to covalently immobilize the GOD onto the particles. By peeling off the stencil, the GOD-modified microparticle pattern was left on the substrate. 50 mM D-glucose dissolved in PBS(−) was dropped onto the GOD pattern to previously initiate the glucose oxidation. Then, the oxygen imaging sheet was put on the GOD pattern to obtain fluorescent image of oxygen-consuming activity.

3. Results and Discussion

Figure 3 shows snapshots over time of the microparticle patterning using electrohydrodynamic force. Microparticles were introduced into the microchannel to be monodispersed (Fig. 3A). Upon application of the AC electric field, the particles rapidly moved toward the exposed ITO rectangular pattern (Fig. 3B). As demonstrated by several researchers, the application of a low frequency AC electric field drives the particles to move in a direction transverse to the field (toward the bottom ITO electrode pattern) via electrohydrodynamic fluid flow, and the particles accumulate in a two-dimensional ordered structure near the electrode surface.[8] Then, the power supply was switched to DC voltage to immobilize the negatively-charged polystyrene particles on the electrode during the solution change from water to a polyacrylamide prepolymer. Figure 3C shows a photograph of the polyacrylamide hydrogel sheet embedded with the rectangular-shaped sensor particle pattern. The particle transfer efficiency from the ITO electrode surface to the hydrogel was almost 100%.

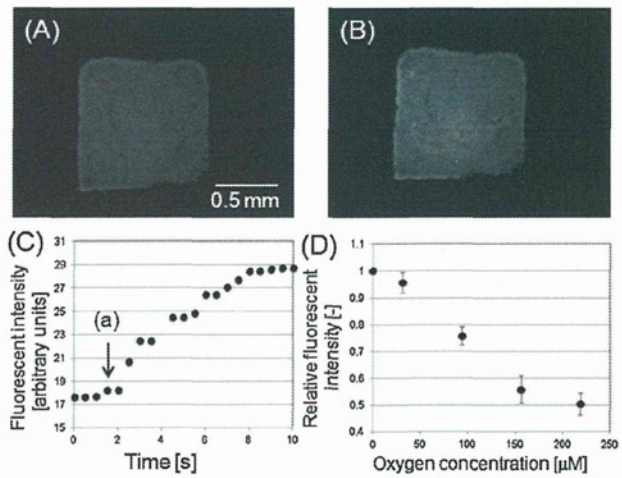

Figure 4. (A, B) Fluorescent images of the oxygen responsive microparticles in PBS(−) at a dissolved oxygen concentration of (A) 185 μM and (B) 0 μM. (C) Typical time-course of the fluorescent intensity change when Na_2SO_3 solution was added into PBS(−) at point (a). (D) Relationship between the relative fluorescent intensity of the imaging sheet and the dissolved oxygen concentration. Oxygen concentration was controlled by gradually adding Na_2SO_3 solution into the previously air-bubbled PBS(−). Each point represents the mean of three measures ± SD.

Figure 4A shows fluorescent images of the oxygen-responsive particles on the hydrogel immersed in PBS(−) dissolving 185 μM oxygen. Oxygen-responsive dye, PtOEP, encapsulated into the particles is based on the ability of molecular oxygen to quench the dye selectively.[9] Therefore, the fluorescent intensity increases as the oxygen concentration decreases. As expected, when Na_2SO_3

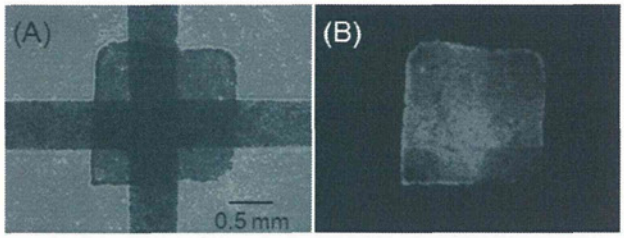

Figure 5. Phase-contrast (A) and fluorescent micrographs (B) of the oxygen imaging sheet attached to the cross-formed GOD-modified microparticles.

(an oxygen scavenger) was added, fluorescent intensity increased (Fig. 4B). 100% response was observed in 6.3 ± 1.2 s after addition of Na_2SO_3 (n = 3, Fig. 4C). Figure 4D shows the inverse relationship between the relative fluorescent intensity of the imaging sheet and the dissolved oxygen concentration measured with a DO meter (Horiba Ltd.). The relative fluorescent intensity indicates the ratio between the fluorescent intensity detected in the absence and the presence of each concentration of oxygen. This result indicated that the gel-sheet can serve as an imaging sensor for dissolved oxygen. The stability of the sensor response was evaluated by measuring the relative fluorescent intensity for PBS(−) every day for a week, showing only 4.2% decrease after 1 week.

Figure 5 demonstrates fluorescent imaging of a GOD-modified microparticle pattern using the oxygen imaging sheet. The imaging sheet was directly attached onto the GOD pattern (Fig. 5A). As can be seen in Fig. 5B, the cross-formed fluorescence displayed corresponds to the GOD pattern. We confirmed there was no response of the imaging sheet against pH change which will be induced by H_2O_2 generation during GOD-catalyzed glucose oxidation. These results suggested that GOD activity was successfully imaged using this patch-type imaging sheet. Non-uniform cross image would be attributed to non-uniform distribution of GOD beads or oxygen sensor beads. Now we are carrying out to optimize electric manipulation of the beads to obtain uniform images.

As mentioned in Introduction, oxygen sensing can be applicable to the study of type 2 diabetes using skeletal muscle cells. Our previous study of scanning electrochemical microscope (SECM) imaging using HeLa cell, which has similar basal respiratory activity with skeletal muscle myoblast,[10] has shown that the difference between the oxygen concentration at the cell surface and the bulk solution far from the cell was ~40 μM.[11] This value corresponds to 0.03 of detectable change in relative fluorescent intensity from the value at bulk oxygen concentration (~200 μM) as estimated from Fig. 4D. The muscle cells enhance their respiratory activities depending on their contractile activities, promising to obtain clear image of contraction-dependent respiratory activity of the cells. During cellular contraction, the sensor beads on the flexible imaging sheet would contract synchronously with the motion of the cells.[12] This characteristic enables continuous monitoring of respiratory activity at same position on the cell surface without concern for disturbance of oxygen concentration gradient around the contracting cells that can cause adverse effect on several oxygen imaging techniques such as SECM.

4. Conclusion

In this study, a patch type oxygen imaging hydrogel sheet was developed. For effective detection of the metabolites in the vicinity of target cells sustaining original hydrogel characteristics, the oxygen sensor beads were locally patterned on the surface of the hydrogel using the electric manipulation technique. We successfully imaged oxygen-consumption activity of GOD pattern as a cellular model, suggesting applicability of the imaging sheet to metabolic bioassays. This flexible sensor sheet is useful for glucose metabolic activity imaging of contracting skeletal muscle cells with supporting cellular contraction to study the relationship between exercise and metabolic activity of muscle in type 2 diabetes.[13]

Acknowledgment

This work was supported by a Core research for Evolutional Science and Technology grant from the Japan Science and Technology Agency.

References

1. M. I. J. Stich, L. H. Fischer, and O. S. Wolfbeis, *Chem. Soc. Rev.*, **39**, 3102 (2010).
2. S. Schreml, R. J. Meier, O. S. Wolfbeis, T. Maisch, R. M. Szeimies, M. Landthaler, J. Regensburger, F. Santarelli, I. Klimant, and P. Babilas, *Exper. Dermat.*, **20**, 550 (2011).
3. S. Schreml, R. J. Meier, O. S. Wolfbeis, M. Landthaler, R. M. Szeimies, and P. Babilas, *Proc. Natl. Acad. Sci. USA*, **108**, 2432 (2011).
4. S. Kimura, K. Matsumoto, K. Mineura, and T. Itoh, *J. Neurol. Sci.*, **258**, 60 (2007).
5. W. Lee, N. J. Cho, A. M. Xiong, J. S. Glenn, and C. W. Frank, *Proc. Natl. Acad. Sci. USA*, **107**, 20709 (2010).
6. X. D. Wang, H. H. Gorris, J. A. Stolwijk, R. J. Meier, D. B. M. Groegel, J. Wegener, and O. S. Wolfbeis, *Chem. Sci.*, **2**, 901 (2011).
7. M. Suzuki, T. Yasukawa, H. Shiku, and T. Matsue, *Langmuir*, **23**, 4088 (2007).
8. K. H. Bhatt, S. Grego, and O. D. Velev, *Langmuir*, **21**, 6603 (2005).
9. K. Montage, K. Komori, F. Yang, T. Tatsuma, T. Fujii, and Y. Sakai, *Photochem. Photobiol. Sci.*, **8**, 1529 (2009).
10. T. C. O'Riordan, A. V. Zhdanov, G. V. Ponomarev, and D. B. Papkovsky, *Anal. Chem.*, **79**, 9414 (2007).
11. M. Nishizawa, K. Takoh, and T. Matsue, *Langmuir*, **18**, 3645 (2002).
12. S. Sekine, Y. Ido, T. Miyake, K. Nagamine, and M. Nishizawa, *J. Am. Chem. Soc.*, **132**, 13174 (2011).
13. K. Nagamine, T. Kawashima, S. Sekine, Y. Ido, M. Kanzaki, and M. Nishizawa, *Lab Chip*, **11**, 513 (2011).

Electrochimica Acta 82 (2012) 175–178

Contents lists available at SciVerse ScienceDirect

Electrochimica Acta

journal homepage: www.elsevier.com/locate/electacta

Sheet-shaped biofuel cell constructed from enzyme-modified nanoengineered carbon fabric

Keigo Haneda [a], Syuhei Yoshino [a], Takuya Ofuji [a], Takeo Miyake [a,b,*], Matsuhiko Nishizawa [a,b,*]

[a] Department of Bioengineering and Robotics, Tohoku University, 6-6-1 Aramaki Aoba, Aoba-ku, Sendai 980-8579, Japan
[b] Core Research for Evolutional Science and Technology (CREST), Japan Science and Technology Agency, Tokyo 102-0075, Japan

ARTICLE INFO

Article history:
Received 27 November 2011
Received in revised form 7 January 2012
Accepted 9 January 2012
Available online 14 February 2012

Keywords:
Biofuel cell
Carbon fabric
Carbon nanotube
Gas-diffusion cathode

ABSTRACT

A strip of carbon fabric (CF) electrode modified with multiwalled carbon nanotubes and subsequently fructose dehydrogenase (FDH) showed an oxidation current density of ~11 mA cm^{-2} in stirred 200 mM fructose solution. Obtaining a sufficient dispersion of the nanotubes during its modification was found to be critical to ensure such a performance of the FDH anode. For use with this anode, a CF strip modified with ketjenblack (KB) and bilirubin oxidase (BOD) served as a gas-diffusion cathode for the reduction of O_2 from air at a current density of ~2 mA cm^{-2}. The FDH-modified CF strip and the BOD-modified CF strip were stacked with an agarose film that retained an electrolyte solution and fuel (fructose) to construct a totally flexible sheet-shaped biofuel cell. This assembly allowed bending of 44° without affecting the maximum output power density, 550 μW cm^{-2} obtained at 0.4 V.

1. Introduction

Enzyme-based biofuel cells that generate electricity through enzymatic oxidation of biological fuels like sugars and alcohols have attracted attention as ubiquitous, safe power sources [1–23]. Recent rapid improvements in their power performance up to mW cm^{-2} levels by employing nanostructured carbon electrodes [24–28] have motivated various applications including a sheet-shaped cell that can be combined with advanced flexible film electronics [29,30]. However, the brittle carbon electrodes, which are generally aggregates of particulate or tubular nanocarbons, often limit the design and uses of such biofuel cells.

In the present work, we have prepared a totally flexible, sheet-shaped biofuel cell by using a carbon fabric (CF) as the flexible, conductive base for the enzyme electrodes. We modified the CF strip with multiwalled carbon nanotubes (CNTs) and fructose dehydrogenase (FDH) for the oxidation of fructose, and with ketjenblack (KB) and bilirubin oxidase (BOD) for the reduction of oxygen in the ambient air. Both FDH and BOD are capable of efficient "direct electron transfer" with common electrode materials including carbon [10,16,21,31,32]. The pre-modifications with CNT or KB increase the specific surface area of the CF electrodes, resulting in effective enzyme immobilization and, ultimately, higher power. The FDH anode strip and the BOD cathode strip are stacked with a hydrogel film that retains the electrolyte solution and fuel (fructose), as shown in Fig. 1. This assembly provides a stand-alone, sheet-shaped power source that can be bent without loss of output power.

2. Experimental

2.1. Preparation of carbon fabric anode

A 5 mm × 5 mm strip of carbon fabric (CF) (TCC-3250, donated from Toho Tenax Co.) was first modified with multiwalled carbon nanotubes (Baytubes, donated from Bayer Material Science Co.) to increase the specific surface area. The carbon nanotubes (CNTs) were pretreated by heating at 400 °C for 11 h and by immersing in mixed acid ($H_2SO_4 + HNO_3$ in a 1:3 ratio) for 5 h. The treated CNT were dispersed in water containing Triton X-100 surfactant (0.05, 0.1, 0.5 or 1%). A 40 μl aliquot of the 10 mg ml^{-1} CNT dispersion was dropped on a CF strip (0.32 mm thickness, 0.25 cm^2 geometric area) and dried in air, followed by thoroughly washing out the surfactant by soaking in a pure McIlvaine buffer solution for more than 1 h with stirring. Then, the CNT-modified CF strip was immersed in a 5 mg ml^{-1} solution of D-fructose dehydrogenase (FDH) (EC1.1.99.11, 169.9 U mg^{-1}, ca. 140 kDa, from Gluconobacter, purchased from Toyobo Enzyme Co.) for FDH immobilization [28]. It has been reported that FDH works as a electrocatalyst for oxidation of fructose without electron transfer mediators [10,16,21,31]. The flavin-containing subunit of FDH accepts electrons from fructose, and transfers these electrons to the heme C-containing subunit that can electrically communicate with electrode [31].

* Corresponding authors at: Department of Bioengineering and Robotics, Tohoku University, 6-6-1 Aramaki Aoba, Aoba-ku, Sendai 980-8579, Japan.
Tel.: +81 22 795 7003; fax: +81 22 795 7003.
E-mail address: nishizawa@biomems.mech.tohoku.ac.jp (M. Nishizawa).

0013-4686/$ – see front matter © 2012 Published by Elsevier Ltd.
doi:10.1016/j.electacta.2012.01.112